Journal of Electronic Research and Application, 2026, Volume 10, Issue 5
http://ojs.bbwpublisher.com/index.php/JERA
Online ISSN: 2208-3510
Print ISSN: 2208-3502

Research on Speed Sensorless Hybrid Control Strategy of Permanent Magnet Synchronous Motor

Shengli Wang*, Wei Liu

School of Electrical and Control Engineering, Jilin University of Chemical Technology, Jinlin, China

Author to whom correspondence should be addressed.

Abstract: In order to obtain the real-time information of the rotor of permanent magnet synchronous motor (PMSM) and improve the accuracy of speed and position estimation of the traditional speed sensorless control strategy of PMSM, a speed sensorless control scheme of PMSM in full speed range was proposed. A PMSM control system based on improved high-frequency injection algorithm and optimized sliding-mode observer is designed. In the low-speed region, the motor position error signal is extracted by the second-order generalized integrator. In the high-speed region, an improved reaching law sliding mode observer combined with a normalized phase-locked loop is used to eliminate the phase delay. In the full speed domain, the smooth weighting function based on the power function is used to dynamically adjust the weighting coefficient to realize the smooth switching of the algorithm. A system simulation model is built in MATLAB/Simulink to verify the effectiveness of the theoretical algorithm. The simulation results show that the hybrid control strategy of PMSM designed in this paper can realize the full-speed operation of PMSM under the conditions of no-load and load operation.

Keywords: Permanent magnet synchronous motor (PMSM); High frequency injection; Motor control; Synovium observer method

Online publication: Jun 29, 2026

1. Introduction

As the core power equipment supporting modern industrial system and daily life, motor plays an increasingly critical role in the wave of electric vehicle driven by energy transformation and “double carbon” goal. The performance of driving motor directly affects the energy efficiency, reliability and driving experience of the whole vehicle, so the selection of motor type has become one of the keys to the technical route of electric vehicle. The traditional DC motor has been difficult to meet the requirements of economy and reliability of electric vehicle because of the problems of brush wear, short life and high maintenance cost [1,2].

In this context, permanent magnet synchronous motor (PMSM) has gradually become the mainstream

choice of electric vehicle drive system because of its high efficiency, high power density and excellent dynamic performance. The invention has the advantages of simple structure and long service life, and due to the adoption of permanent magnet excitation, an excitation circuit is omitted, and the efficiency is obviously improved [3]. In addition, China is rich in rare earth resources, which provides favorable conditions for the promotion and application of permanent magnet motors. At present, vector control technology is widely used in PMSM control system, which highly depends on the real-time speed and rotor position information provided by the speed sensor. The more accurate the feedback, the better the control. However, sensors are not only expensive, but also vulnerable to interference and high failure rate, which directly affect the safety and reliability of the system.

In order to overcome the limitations brought by the sensor, the speed sensorless control method has become a hot research topic at home and abroad [4]. The method aims at estimating the rotating speed and the rotor position through a motor mathematical model and electrical parameters, so that a physical sensor is omitted in hardware, and the purpose of reducing cost and increasing efficiency is achieved. However, each of the existing single type of sensorless methods has its limitations: for example, the synovial membrane observer method has excellent performance in the medium-high speed region, but the observation accuracy decreases at low speed due to the small back electromotive force. Although the high frequency voltage signal injection method is suitable for the zero low speed range, it will introduce additional noise and reduce the voltage utilization of the inverter.

In view of the above problems, this paper focuses on the performance optimization of speed sensorless control of permanent magnet synchronous motor, and studies how to integrate the advantages of different methods to construct a composite control strategy that can maintain good performance in a wide speed range [5]. By intelligently switching a sliding mode observer method and a high-frequency injection method under different working conditions, a smooth weighting function based on a power function is adopted, and the two control strategies are combined to solve the problems that the high-frequency voltage injection method is not suitable for long-time operation of the motor, the sliding mode observer method has large low-speed observation error and the like, Global stable estimation and control from zero speed to high speed is realized. This study has important theoretical value and engineering significance for improving the comprehensive performance, reducing the cost and improving the reliability of the electric vehicle drive system [6].

2. System structure design and method

The basic principle of the high-frequency pulsating signal injection method is to inject a high-frequency sinusoidal voltage signal into the d-axis of the estimated rotor synchronous rotating coordinate system, and then detect the high-frequency current response generated by the stator side, which encodes the error information between the actual position and the estimated position of the rotor [7]. The position error is extracted from the current by a filter and a demodulation algorithm, and the estimated value is continuously corrected by using the position error, so that the position and the rotating speed of the rotor are accurately estimated in real time, and the stable operation of the sensorless rotor is realized.

2.1. Design of traditional pulsating high-frequency voltage injection method

In the dq coordinate system, the PMSM voltage equation is:

$$\begin{bmatrix} u_d \\ u_q \end{bmatrix} = \begin{bmatrix} R_s + pL_d & -\omega_e L_q \\ \omega_e L_d & R_s + pL_q \end{bmatrix} \begin{bmatrix} i_d \\ i_q \end{bmatrix} + \begin{bmatrix} 0 \\ \omega_e \varphi_f \end{bmatrix} \tag{1}$$

Among them, u_d and u_q are the dq-axis voltage components; i_d and i_q are the dq-axis current components; R_s is the stator resistance; L_D, L_q dq axis inductances, respectively; ω_e is the electric angular velocity; φ_f is a permanent magnet magnetic chain.

The traditional method is based on the magnetic-saturation saliency effect of salient-pole PMSM. A high frequency sinusoidal voltage signal is inject on that DQ direct axis of the estimated rotate frame:

$$\begin{bmatrix} \hat{u}_{dh} \\ \hat{u}_{qh} \end{bmatrix} = \begin{bmatrix} V_h \cos(\omega_h t) \\ 0 \end{bmatrix} \tag{2}$$

Among, V_h for the magnitude of the injection voltage, ω_h is the injection angular frequency. Due to the saliency of the motor, the injected voltage will be q. The shaft generates an error signal containing rotor position information $\Delta\theta$. High frequency current component of:

$$\begin{bmatrix} i_{dh} \\ i_{qh} \end{bmatrix} \approx \begin{bmatrix} \dfrac{V_h}{\omega_h L_d} \sin(\omega_h t)\cos\Delta\theta \\ -\dfrac{V_h}{\omega_h L_q} \sin(\omega_h t)\sin\Delta\theta \end{bmatrix} \tag{3}$$

After conversion to the dq estimation coordinate system and simplification, the q-axis high-frequency response current containing the position error is:

$$i_{qh} = I_{h1} \sin(\omega_h t)\sin(2\Delta\theta) \approx I_{h1} \sin(\omega_h t) \cdot 2\Delta\theta \tag{4}$$

Here I_{h1} is the magnitude coefficient affected by the inductance saliency.

Multiplying the extracted signal by the same frequency signal of the injected carrier is:

$$f(\Delta\theta) = i_{qh} \cdot \sin(\omega_h t) = I_{h1} sin^2(\omega_h t)\sin(2\Delta\theta) \tag{5}$$

Using the trigonometric identity $sin^2 x = \dfrac{1-\cos(2x)}{2}$, available:

$$f(\Delta\theta) = \frac{1}{2} I_{h1} \sin(2\Delta\theta) \quad -\frac{1}{2} I_{h1} \cos(2\omega_h t)\sin(2\Delta\theta) \tag{6}$$

The 2-fold high-frequency term needs to be filtered out

Filtered by low-pass filter $2\omega_h$ Section, and normalized (i.e., divided by the amplitude of the high frequency current I_h) to obtain the final angle error signal for the closed loop:

$$\varepsilon = \mathrm{LPF}\left[f(\Delta\theta) \right] \approx \Delta\theta \tag{7}$$

The error signal ε into the PLL structure. The position is calculated as:

$$\hat{\theta}_c = \frac{1}{s} \hat{\omega}_c \tag{8}$$

The speed is calculated as:

$$\hat{\omega}_c = \left(K_p + \frac{K_i}{s} \right) \cdot \varepsilon \tag{9}$$

As shown in **Figure 1**, this shows how speed and position information is extracted by the conventional pulsating high frequency voltage injection method.

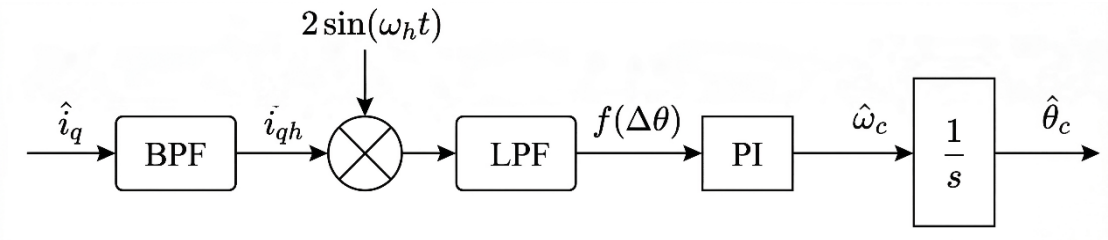

Figure 1. Extraction of speed and position information by traditional pulsating high frequency voltage injection method.

2.2. Improved high frequency injection design

The filter will limit the bandwidth of the current loop and the speed loop, thus reducing the filtering accuracy of the system. In this paper, SOGI is introduced to replace the traditional filter to improve the accuracy of rotor position observation [8].

The SOGI can be regarded as a special ultra-narrow passband BPF, which has a simple structure and only needs two integrators plus a feedback loop. Owing to its closed-loop feedback structure, the SOGI can accurately lock and extract the given center frequency, and simultaneously generate two outputs in phase and quadrature with the input signal, which is convenient for position information demodulation. The structure of SOGI is shown in **Figure 2**.

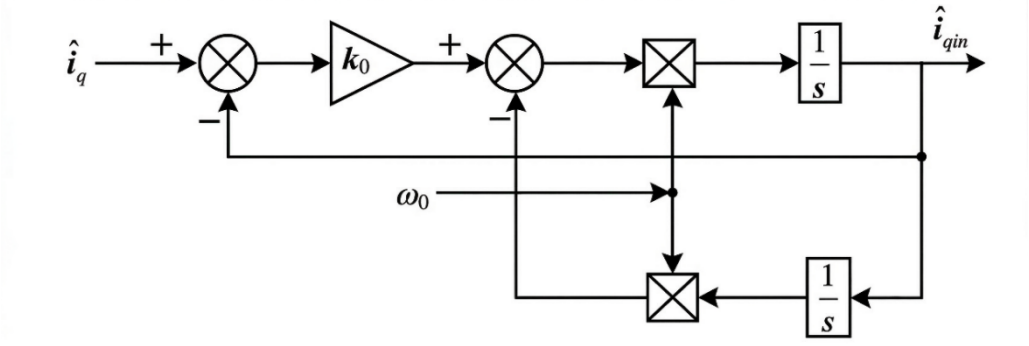

Figure 2. Structure diagram of SOGI.

The transfer function of SOGI is:

$$G_{SOGI}(s) = \frac{k\omega_0 s}{s^2 + k\omega_0 s + \omega_0^2} \tag{10}$$

The feedback current signal $\hat{i}_q$ enter SOGI, k is the gain factor, ω_0 is the center frequency. Fundamental wave $v = i_{qh}$, then the quadrature output qv:

In the improved pulsating high-frequency voltage injection method, as shown in **Figure 3**, two SOGIs (Phase-Locked Loops) are used to extract high-frequency signal components and position error information.

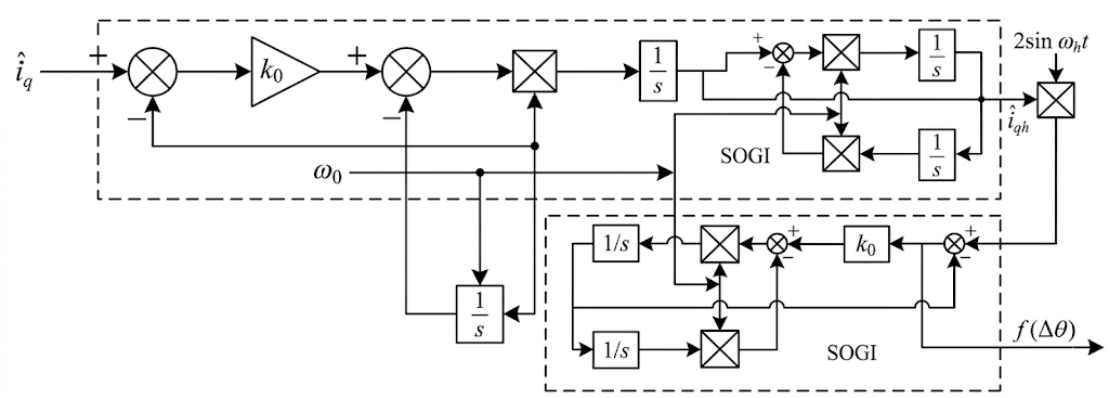

Figure 3. Block diagram of improved pulsating high frequency voltage injection method for location information extraction.

The position error signal after SOGI processing is:

$$f\left(\Delta\theta\right)=\mathrm{SOGI}\left\{\mathrm{SOGI}\left(\hat{i}_q\right)\cdot 2\sin\omega_h t\right\}=\frac{u_h\left(L_q-L_d\right)}{2\omega_h L_d L_q}\sin(2\Delta\theta)=k_e\sin(2\Delta\theta) \tag{11}$$

After the position error signal is extracted, the position information of the motor rotor is obtained through a phase-locked loop. As shown in **Figure 4**, this paper uses two Second-Order Generalized Integrators (SOGIs) to extract signal components and motor position error.

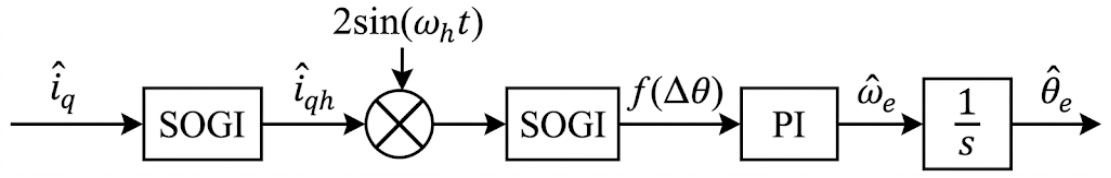

Figure 4. Block diagram of improved pulsating high frequency voltage injection method for position estimation.

When the system is near the equilibrium point, we have $\Delta\theta=\theta_e-\hat{\theta}_e$.

The closed-loop transfer function of the phase-locked loop :

$$G_{\mathrm{PLL}}\left(s\right)=\frac{\hat{\theta}_e}{\theta_e}=\frac{K_p s+K_i}{s^2+K_p s+K_i}=\frac{2\xi\omega_n s+\omega_n^2}{s^2+2\xi\omega_n s+\omega_n^2} \tag{12}$$

Among $K_p=2\xi\omega_n$, $K_i=\omega_n^2$. The speed of the rotor can be obtained by PI calculation, and the position of the rotor can be obtained by integration. The block diagram of the improved high frequency voltage injection method is shown in Fig**ure 5**.

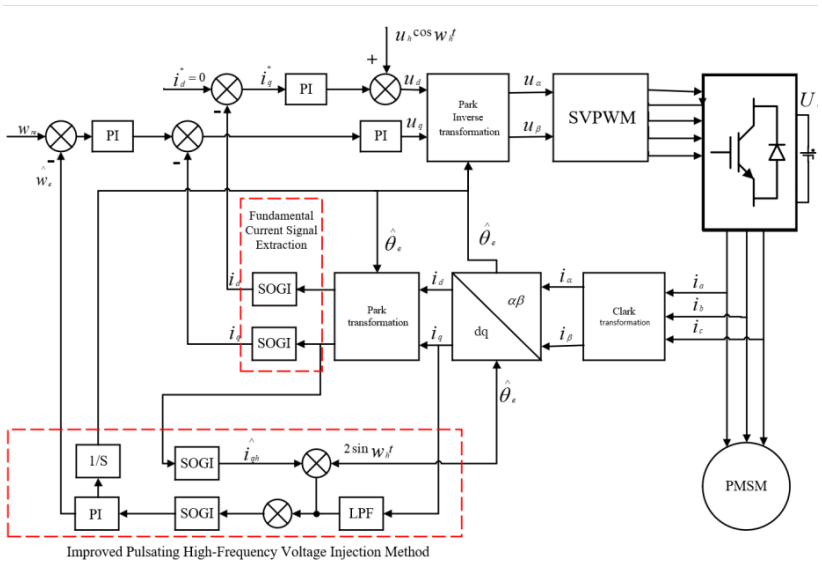

Figure 5. Overall control schematic diagram of improved high frequency pulse voltage injection.

2.3. Design of the synovial membrane observer

A mathematical model of a conventional slide mode observer under the axis is:

$$\begin{cases} u_\alpha = R_s i_\alpha + L_s \dfrac{di_\alpha}{dt} + e_\alpha \\ u_\beta = R_s i_\beta + L_s \dfrac{di_\beta}{dt} + e_\beta \end{cases} \tag{13}$$

Among, $\begin{cases} e_\alpha = -\omega_e \psi_r \sin\theta \\ e_\beta = -\omega_e \psi_r \cos\theta \end{cases}$, e_α、e_β, for $\alpha\beta$, the component of the electromotive force under the shaft, ω_e is the electrical angular velocity, θ is the electrical angle. An equation of state for the current can be derived:

$$\begin{cases} \dfrac{di_\alpha}{dt} = \dfrac{u_\alpha}{L_s} - \dfrac{e_\alpha}{L_s} - \dfrac{R_s i_\alpha}{L_s} \\ \dfrac{di_\beta}{dt} = \dfrac{u_\beta}{L_s} - \dfrac{e_\beta}{L_s} - \dfrac{R_s i_\beta}{L_s} \end{cases} \tag{14}$$

Assuming $u(x)$=Ksign(x), K Gain for synovium.

The switching function is:

$$s(x) = \begin{cases} \hat{i}_\alpha - i_\alpha \\ \hat{i}_\beta - i_\beta \end{cases} \tag{15}$$

The control function is:

$$sign(x) = \begin{cases} 1 & x > 0 \\ 0 & x = 0 \\ -1 & x < 0 \end{cases} \tag{16}$$

The error function between the actual position and the estimated position of the stator is:

$$\begin{cases} \hat{i}_\alpha = i_\alpha - i_\alpha \\ \tilde{i}_\beta = \hat{i}_\beta - i_\beta \end{cases} \tag{17}$$

Then the current error equation is:

$$\begin{cases} \dfrac{d\tilde{i}_\alpha}{dt} = -\dfrac{R_s \tilde{i}_\alpha}{L_s} - \dfrac{K}{L_s} sign\left(\tilde{i}_\alpha\right) + \dfrac{e_\alpha}{L_s} \\ \dfrac{d\tilde{i}_\beta}{dt} = -\dfrac{R_s \tilde{i}_\beta}{L_s} - \dfrac{K}{L_s} sign\left(\tilde{i}_\beta\right) + \dfrac{e_\beta}{L_s} \end{cases} \tag{18}$$

Construct the sliding surface S :

$$S = \begin{bmatrix} S_\alpha \\ S_\beta \end{bmatrix} = \begin{bmatrix} \hat{i}_\alpha - i_\alpha \\ \hat{i}_\beta - i_\beta \end{bmatrix} = \begin{bmatrix} \tilde{i}_\alpha \\ \tilde{i}_\beta \end{bmatrix} \tag{19}$$

Because $S = S = 0$, then:

$$\begin{cases} S_\alpha = \hat{i}_\alpha - i_\alpha = \dfrac{d\left(\hat{i}_\alpha - i_\alpha\right)}{dt} = 0 \\ S_\beta = \hat{i}_\beta - i_\beta = \dfrac{d\left(\hat{i}_\beta - i_\beta\right)}{dt} = 0 \end{cases} \tag{20}$$

So the components of the back EMF are:

$$\begin{cases} e_\alpha = ksign\left(\hat{i}_\alpha - i_\alpha\right) \\ e_\beta = ksign\left(\hat{i}_\beta - i_\beta\right) \end{cases} \tag{21}$$

In order to eliminate the high frequency vibration phenomenon, the low pass filter is quoted as:

$$\begin{cases} \hat{e}_\alpha = \dfrac{\omega_c}{s + \omega_c} e_\alpha \\ \hat{e}_\beta = \dfrac{\omega_c}{s + \omega_c} e_\beta \end{cases} \tag{22}$$

The rotor position angle is:

$$\hat{\theta}_{eq} = -\arctan\left(\frac{\hat{e}_\alpha}{\hat{e}_\beta}\right) \tag{23}$$

Differentiate the angle to get ω_e , so the speed estimate $\hat{\omega}_e$:

$$\hat{\omega}_e = \frac{\sqrt{\hat{e}_\alpha^2 + e_\beta^2}}{\psi_f} \tag{24}$$

After filtering, the phase of the back EMF estimation component may lag behind, and an angle compensation term is added to correct the position angle estimation deviation caused by the delay effect of the low-pass filter, that is:

$$\hat{\theta}_e = \theta_{eq} + \arctan(\hat{\omega}_e / \omega_c) \tag{25}$$

The block diagram of the traditional sliding mode observer system is as follows (**Figure 6**):

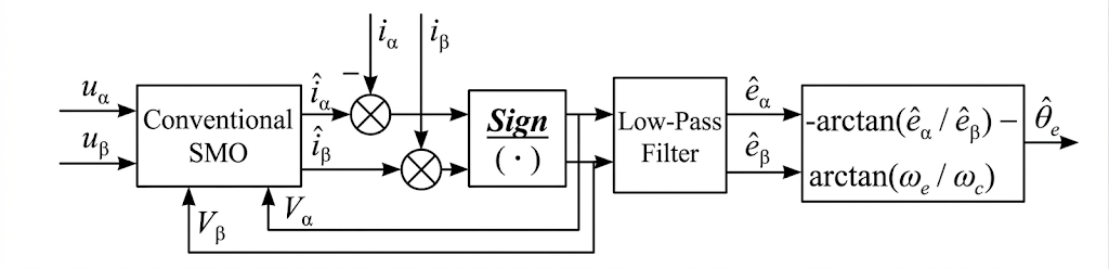

Figure 6. System block diagram of conventional sliding mode observer.

Although the traditional sliding mode observer can realize the sensorless control of the motor, the discontinuity of the core sign function will cause the system chattering, which will lead to the high-frequency error of the estimated back EMF and the phase delay caused by the low-pass filter introduced to filter the error [9]. Especially in high-speed conditions, the control effect is seriously affected, and the forced phase compensation will increase the amount of calculation and reduce the response speed.

2.4. Improved synovial observer design

In this paper, an improved sliding mode observer is proposed, which uses an improved reaching law to weaken the chattering smooth signal from the control source, and replaces the sign function to make the sliding mode motion as close as possible to the ideal sliding mode motion. A phase-locked loop is introduced to replace the traditional filter and arctangent structure, so that the phase delay is eliminated, the accuracy of rotor position and speed estimation and the overall stability of the system are improved.

In this paper, the sigmoid function is chosen to replace the sign function as the control function. After replacing the control function, a new reaching law is obtained as follows:

$$u(x) = \text{KSigmoid}(x) \tag{26}$$

The new sliding mode observer is given by:

$$\begin{cases} \dfrac{d}{dt}\hat{i}_\alpha = -\dfrac{R_s}{L_d} i_\alpha - \omega_e \dfrac{L_d - L_q}{L_d} i_\beta + \dfrac{u_\alpha}{L_d} - \dfrac{v_\alpha}{L_d} \\ \dfrac{d}{dt}\hat{i}_\beta = -\dfrac{R_s}{L_d} i_\beta + \omega_e \dfrac{L_d - L_q}{L_d} i_\alpha + \dfrac{u_\beta}{L_d} - \dfrac{v_\beta}{L_d} \end{cases} \tag{27}$$

The components of the off-axis back EMF are:

$$\begin{cases} e_\alpha = ksigmoid\left(\hat{i}_\alpha - i_\alpha\right) \\ e_\beta = ksigmoid\left(\hat{i}_\beta - i_\beta\right) \end{cases} \tag{28}$$

In the traditional sliding mode observer, in order to convert the back electromotive force information of the motor into the information of the motor speed and the rotor position, the arc tangent operation is carried out, but the arc tangent operation has adverse effects on the whole control system and increases the system chattering. Therefore, this paper uses the phase-locked loop instead of the arctangent function to calculate the motor rotor position, and normalizes it. The structure of the phase-locked loop normalization is as shown in **Figure 7**:

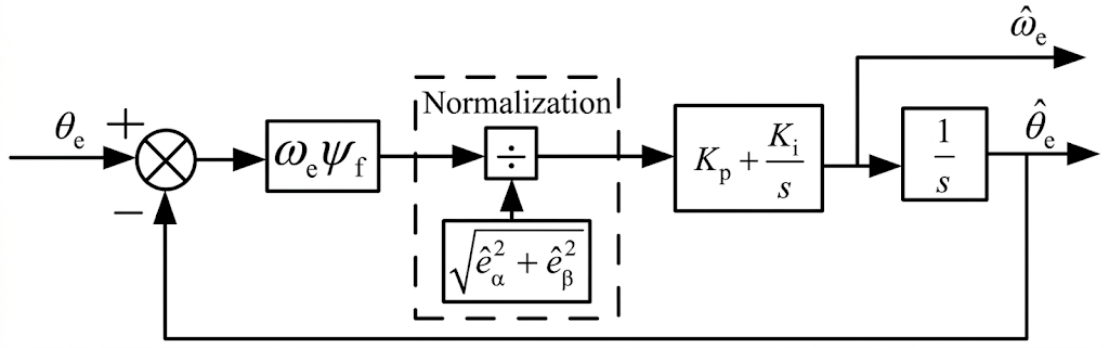

Figure 7. Phase locked loop normalization schematic.

A surface-mounted permanent magnet synchronous motor is selected, assuming that $k = \hat{\omega}_e \psi_f$, the error signal can be obtained ΔE :

$$\begin{aligned} \Delta E &= -\hat{e}_\alpha \cos\hat{\theta} - e_\beta \sin\theta \\ &= k\sin\theta\cos\hat{\theta} - k\cos\theta\sin\theta \\ &= k\sin(\theta - \hat{\theta}) \end{aligned} \tag{29}$$

When the angle error $\left|\theta - \hat{\theta}\right| < \pi/6$, according to the linearized approximation $\sin(\theta - \hat{\theta}) \approx \theta - \theta \approx \varepsilon$ available:

$$\Delta E = k\sin(\theta - \hat{\theta}) \approx k\left(\theta - \hat{\theta}\right) \tag{30}$$

The normalized error ε is sent to the PI controller, and the output of the PI is the estimated electrical angular velocity.

$$\hat{\omega}_e = \left(K_p + \frac{K_i}{s}\right) \cdot \varepsilon \tag{31}$$

Finally, the estimated angular velocity $\hat{\omega}_e$, the final rotor position information can be obtained by time integration.

$$\hat{\theta}_e = \int \hat{\omega}_e dt = \frac{1}{s}\hat{\omega}_e \tag{32}$$

The normalized phase-locked loop system uses the PI controller to achieve the accurate acquisition of the rotor position information. At the same time, the rotor speed value can be calculated by integral operation, which effectively inhibits the potential interference of high-frequency signals, thus ensuring the stability and accuracy of the system. The design diagram of the optimized sliding mode observer is shown in **Figure 8**:

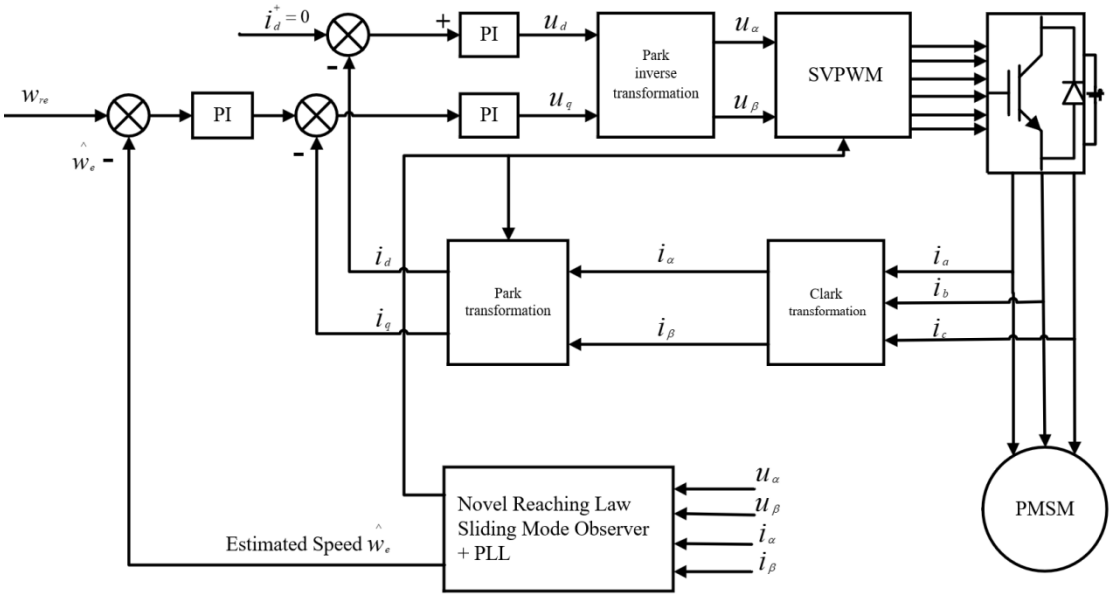

Figure 8. Schematic diagram of optimal sliding mode observer design.

2.5. Control switching strategy

In order to achieve reliable sensorless operation of permanent magnet synchronous motor (PMSM) in the full speed range, the system needs a smooth transition between different control algorithms according to the motor speed [10]. Usually, the high frequency injection method is used to obtain better rotor position estimation accuracy at zero low speed condition. In the case of medium and high speed, the sliding mode observer (SMO) algorithm is used. This state transition process from low speed to high speed is the control switching strategy.

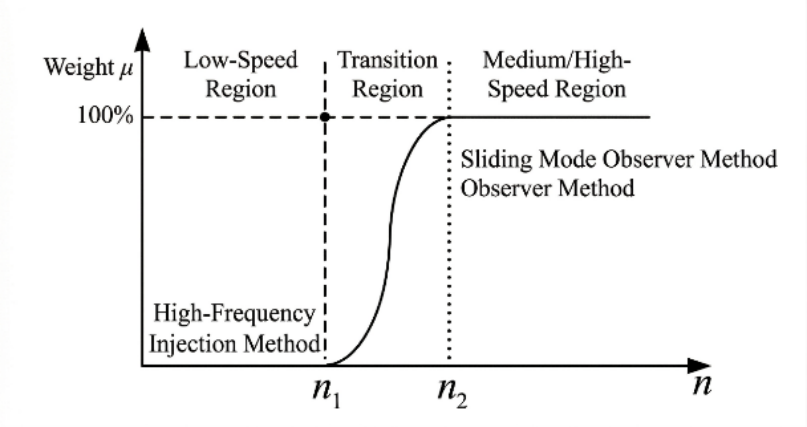

Figure 9. Weighted switching schematic.

2.5.1. Weighted switching principle

The system introduces a transition interval [n_1, n_2] To achieve the fusion of the two algorithms, such as **Figure 9**. The ordinate represents the weighting coefficients of the algorithm, which reflects the mapping relationship between the speed and the weight. In the low speed regio, the system completely adopts the high frequency injection method. At a transition zone, the final estimated motor speed and rotor position information are obtained by the weighted average of the results of the two algorithms. As the speed increases, the weight of the sliding mode observer increases. Finally, in the middle and high speed area, the system is completely switched to the sliding mode observer method.

2.5.2. Improved smoothing weighted switching function

Although the traditional linear weighted switching is able to achieve the basic transition, at the switching start point, n_1 and the end n_2. The sudden change of the slope will cause the transition to be harsh, which will still have a slight impact on the stability of the system.

In order to obtain a better control effect, this paper improves the weight function and introduces a power function curve instead of a linear curve to achieve a smoother weighted switching.

The expression of the improved smooth weighted weight function is as follows:

$$\mu(n)=\begin{cases} 2^{a-1}\left(\dfrac{n-n_1}{n_2-n_1}\right)^a & n_1 < n \le \dfrac{n_1+n_2}{2} \\ 1-2^{a-1}\left(1-\dfrac{n-n_1}{n_2-n_1}\right)^a & \dfrac{n_1+n_2}{2} < n \le n_2 \end{cases} \tag{33}$$

By adjusting the exponent of the power function *a*, The bending degree of the weight curve can be flexibly changed. Compared with the linear function, the proposed function is smoother at the switching boundary, which can further reduce the torque and speed fluctuations in the switching process and enhance the robustness of the control system.

3. Simulation analysis of compound control motor control system

3.1. Motor operation simulation experiment with fusion algorithm

The simulation model of the PMSM controlled using the improved high-frequency injection algorithm and the optimized sliding-mode observer algorithm is shown in **Figure 10**.

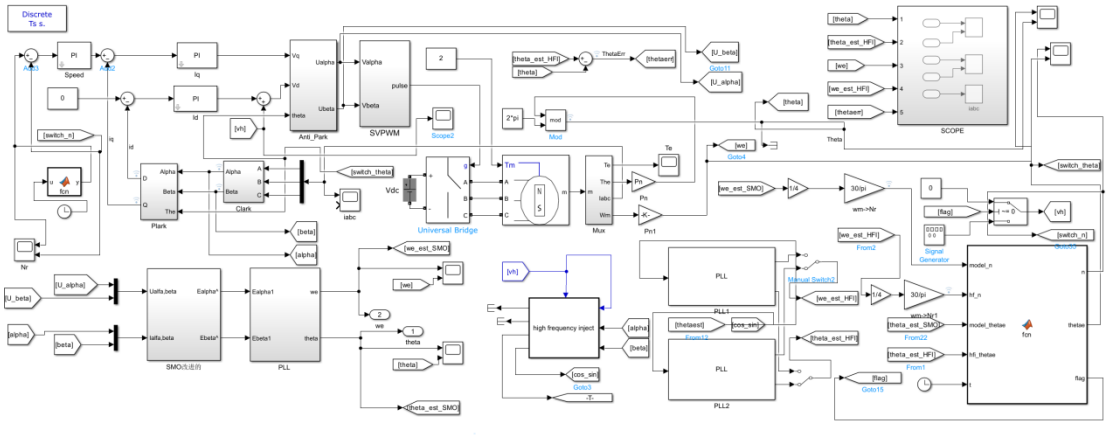

Figure 10. Simulink simulation model of fusion algorithm.

After the application of the fusion algorithm, as shown in **Figure 11**, it can be observed from the waveform that the three-phase current waveforms have a 120-degree phase difference between the three-phase sine waves. The current waveform is relatively smooth, the stability is good, and the motor can operate normally in this simulation system.

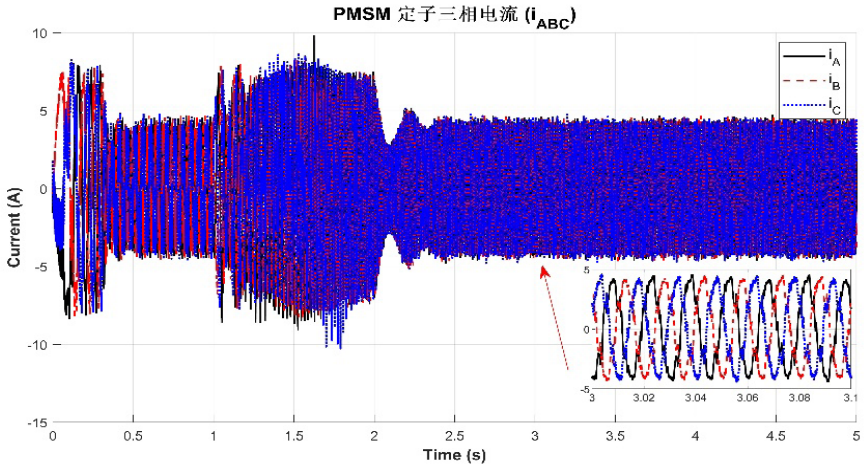

Figure 11. Three-phase current waveform.

The rotor position angle tracking of the motor rotation observation estimated by the fusion algorithm is shown in **Figure 12**:

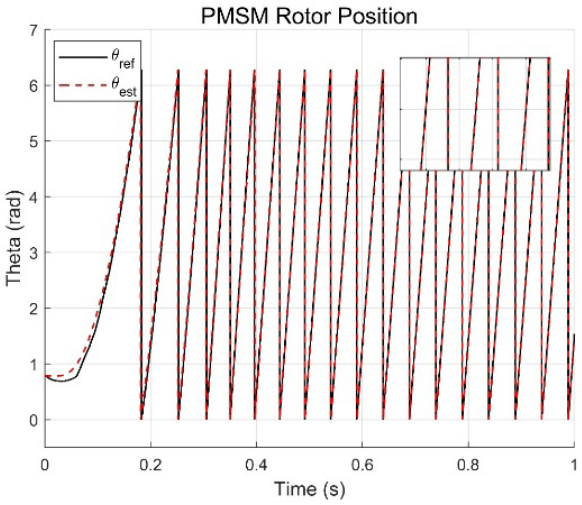

Figure 12. Rotor position tracking diagram.

The curve represents the actual position of the rotor when the motor is running, and the red curve represents the rotor position estimated by the fusion algorithm. The fusion algorithm can achieve fast convergence in about 0.15 seconds, and the estimated position is almost perfectly coincident with the actual position in all the following periods, which shows that the fusion algorithm has extremely high steady-state tracking accuracy.

As shown in **Figure 13**, this is a perfect example of the motor switching from low-speed operation (300 rpm) to high-speed operation (1000 rpm). From the steady-state performance, the algorithm achieves a high degree of coincidence between the estimated value and the actual reference value in the low speed range of 300 rpm and the high speed range of 1000 rpm, and the steady-state tracking error is close to zero, which proves its extremely high accuracy of position and speed estimation under different working conditions.

At the 1.0s switching point, the system is subject to a small disturbance (the actual speed drops for a short time), but the estimated speed catches up and locks quickly, and it only takes about 0.2s from the disturbance to the stable tracking again. This smooth transition mechanism effectively avoids the angle jump, and fully verifies the reliability of the fusion strategy in the full speed range and the extremely fast dynamic response within 0.2s.

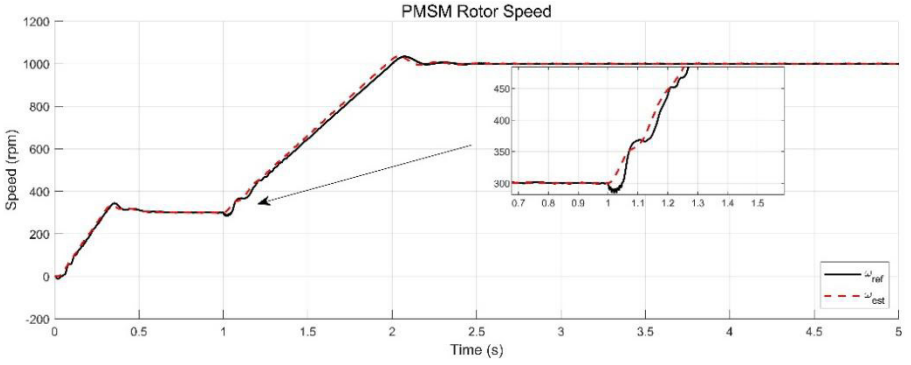

Figure 13. Application of fusion algorithm to motor waveform in full speed ran.

4. Conclusion

In this paper, the improved pulsating high frequency voltage injection method and the optimized sliding mode observer are applied to the permanent magnet synchronous motor (PMSM) control system, and the MATLAB/Simulink simulation model of the sensorless vector control system based on the composite algorithm is built. The simulation results show that the improved high frequency injection and optimal sliding mode algorithm has excellent performance in speed tracking and rotor position tracking experiments at low speed and medium and high speed. Its tracking waveform is smooth and stable, and it has high anti-interference ability and robustness, which meets the real-time requirements of motor control and realizes the stable operation of the motor in the full speed range.

Disclosure statement

The authors declare no conflict of interest.

References

[1] Chen Z, 2025, Research on Performance Optimization Control Technology of Permanent Magnet Synchronous Motor Drive System, thesis, University of Electronic Science and Technology of China.

[2] Ren D, 2023, Research on PMSM Control Method based on Position Sensorless Algorithm, thesis, Beijing Jiaotong University.

[3] Du J, Liu B, Yang X, et al., 2025, Dynamic Analysis of Rotor and Machine Structure in Ultra-High-Speed PMSM. International Journal of Simulation Modelling, 24(3).

[4] Wu Z, Wang D, Zhao Y, et al., 2025, Analysis and Optimization of Electromagnetic Characteristics of Asymmetric V-Shaped Interior Permanent Magnet Synchronous Motor. Journal of Electrical Engineering & Technology, 2025.

[5] Tan F, Ma Y, Zhao C, 2025, Research on Speed Control of PMSM Based on Super-Twisting Sliding Mode Corrected Differential Linear Active Disturbance Rejection. Energies, 18(17).

[6] Abdellatif W, Saleh A, Salem A, et al., 2025, Wind-Speed Estimation Maximum Power Point Tracking Scheme for Permanent Magnet Synchronous Machine-based Wind Energy Conversion Systems. Journal of Power Electronics, 2025.

[7] Zheng L, Zuo D, 2025, Suppression of Periodic Speed Disturbances in Permanent Magnet Synchronous Motors based on Sliding Adaptive Filters. Journal of Physics: Conference Series, 3097(1).

[8] Lan C, 2025, Simulink Modeling of Dual-Loop Speed Control for Permanent Magnet Synchronous Motors. Journal of Engineering Research and Reports, 27(9).

[9] Chen J, 2024, Research on Sensorless Control Algorithm of Full-speed PMSM Based on SOGIFO-X, thesis, Dalian University of Technology.

[10] Chen H, 2025, Sensorless Control of Permanent Magnet Synchronous Motor based on High Frequency Square Wave Injection. Internet of Things Technology, 15(17): 80–84.